LBNL-44898
Preprint

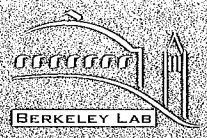

ERNEST ORLANDO LAWRENCE
BERKELEY NATIONAL LABORATORY

Three-Dimensional Position Sensing and Field Shaping in Orthogonal-Strip Germanium Gamma-Ray Detectors

M. Amman and P.N. Luke

Engineering Division

January 2000

Submitted to
Nuclear Instruments and Methods in Physics Research — Section A

LBNL-44898

Three-Dimensional Position Sensing and Field Shaping in Orthogonal-Strip Germanium Gamma-Ray Detectors

M. Amman and P.N. Luke

Engineering Division
Ernest Orlando Lawrence Berkeley National Laboratory
University of California
Berkeley, California 94720

January 2000

This work was supported by the Environmental Management Science Program, Office of Science and Technology, Office of Environmental Management, of the U.S. Department of Energy under Contract No. DE-AC03-76SF00098.

Three-Dimensional Position Sensing and Field Shaping in Orthogonal-Strip Germanium Gamma-Ray Detectors[1]

M. Amman*, P. N. Luke

Ernest Orlando Lawrence Berkeley National Laboratory, University of California, Berkeley, California 94720, USA

Abstract

We have fabricated a prototype orthogonal-strip germanium detector for gamma-ray imaging studies. With this detector we demonstrate that a gamma-ray interaction event in the detector can be located in three dimensions. In particular we determine the interaction depth from the difference in time in the arrival of the holes at an electrode on one side of the detector and the arrival of the electrons at an electrode on the opposing detector surface. This depth of interaction sensing should lead to improved image resolution. A separate issue with such a detector is the loss of energy resolution and efficiency resulting from incomplete charge collection for interaction events taking place in the gap regions between the detector electrodes. We also demonstrate with our prototype detector that this problem can be substantially reduced by using field-shaping electrodes. A bias applied between the charge-sensing electrodes and the field-shaping electrodes improves the charge collection to the charge-sensing electrodes and consequently the detector performance.

Suggested PACS: 29.40.Wk; 29.40.Gx; 07.85.+n

Keywords: gamma-ray imaging; gamma-ray spectroscopy; germanium detector; orthogonal strip; position sensing; field shaping

*Corresponding author. Tel.: +1 510 486 5638; fax: +1 510 486 5857; e-mail: Mark_Amman@lbl.gov.

[1]This research was supported in full under Contract No. DE-AC03-76SF00098, Environmental Management Science Program, Office of Science and Technology, Office of Environmental Management, United States Department of Energy (DOE). However, any opinions, findings, conclusions, or recommendations expressed herein are those of the authors' and do not necessarily reflect the views of DOE.

1. Introduction

Gamma-ray imaging with good spatial and energy resolution combined with high detection efficiency is required for many applications including those for astronomy, environmental remediation, and nuclear safeguards monitoring. High-purity germanium (Ge) detectors with their excellent energy resolution and efficiency could potentially fulfill these needs. However, the production of position-sensitive Ge detectors with fine spatial sensitivity has been a significant technical challenge. Even so, substantial progress has been made in the development of these detectors [1-11]. One advancement has been the amorphous semiconductor contact technology [10-13]. This technology offers the advantages of producing contacts that have thin dead layers, can be fine-pitched, and exhibit good blocking behavior under either bias polarity. Furthermore, the fabrication process is simple and automatically produces a passivated surface between the contact segments.

The amorphous semiconductor contact technology enables the simple production of the fine-pitched electrical contacts needed to achieve high spatial resolution. However, the spatial resolution and image quality obtained with a Ge detector are dependent on more than simply the physical segmentation of the detector contacts. The physics of the gamma-ray interaction also plays a role. A gamma-ray will interact at a random depth and potentially multiple times in the detector. In planar-geometry position-sensitive Ge detectors, position detection is normally made in only the directions parallel to the segmented contact surfaces and not in the depth direction. Consequently, parallax image broadening can result. In part to address this problem, we have fabricated a prototype 5×5 orthogonal-strip Ge gamma-ray detector using the amorphous semiconductor contact technology. With this detector, we have investigated the spatial detection of gamma-ray interaction events in the detector in all three dimensions. The depth of interaction in this detector is obtained from the difference in the arrival time of the holes at an electrode on one side of the detector and that of the electrons at an electrode on the opposing detector surface. This separate detection of the hole collection and the electron collection is fundamental to the technique and is facilitated by the small electrode effect [14-16] achieved with the strip electrodes.

Another potential problem is that of incomplete charge collection as a result of the electrical contact segmentation. We show that for some interaction events in our prototype detector the

charge is not completely collected within the signal measurement time as a result of charge collection to the detector surfaces between contact segments. One way to ameliorate this situation is to add an electrode (field-shaping electrode) between each charge-sensing electrode. By applying the appropriate bias between the charge-sensing electrodes and the field-shaping electrodes, efficient collection to the charge-sensing electrodes can be insured. The bipolar blocking nature of the amorphous contacts allows such a biasing configuration to be easily implemented.

In this paper we present the results of our experimental investigation into gamma-ray interaction detection in three dimensions and the use of field-shaping electrodes to improve charge collection and ultimately detector energy resolution and efficiency.

2. Detector design, fabrication, and measurement configuration

The prototype detector used in this study is of an orthogonal-strip design and is schematically shown in Figure 1. The overall size of the detector is about 25 mm × 25 mm × 11 mm thick. The position-sensitive volume of this detector approximately consists of the overlap region between the two sets of strip electrodes on the front and back detector surfaces. Since this is a prototype detector, the electrode design is simple with only five 10 mm long strips of 0.5 mm width and spacing on each side of the detector. A larger than necessary guard ring surrounds each set of strips in order to minimize the potential deleterious effects of surface channels [17] and excessive leakage along the side surfaces. Deep grooves have also been cut into the detector in order to form undepleted and inactive side lobes. These side lobes facilitate detector handling during fabrication and detector mounting in a test fixture.

The starting high-purity Ge material for this detector was p-type with a net impurity concentration of about 4×10^{9} cm^{-3}. To produce the detector, this crystal was first cut into the geometry shown in Figure 1 using a diamond saw. Each of the exposed surfaces of the cut crystal was then lapped in order to remove the blade marks caused by the cutting operation. The surface damage introduced by these mechanical processes was then removed by etching the crystal in a 4:1 nitric to hydrofluoric acid mixture. Following this, the crystal was briefly etched again in fresh 4:1 etchant, quenched in methanol, and blown dry with nitrogen in order to prepare the surfaces for contact deposition. The crystal was then immediately loaded into a RF

sputtering system. Amorphous Ge (a-Ge) was deposited in pure argon at a pressure of 7 mtorr to an approximate 100 nm thickness on the crystal. The crystal was placed front side down in the chamber so that the back and side detector surfaces were coated. Subsequent to this, metal layers forming the strip electrodes and guard ring were deposited on top of the a-Ge layer on the back-side detector surface using thermal evaporation through shadow masks. The metallization consisted of a chromium layer about 25 nm thick to act as an adhesion layer followed by multiple gold evaporations in order to achieve a final electrode thickness of about 500 nm. This metallization scheme was found to produce good results with the wire bonding process used later to make electrical connection to these electrodes. The fabrication process was continued by masking the completed back-side surface with an acid and alcohol resistant cement and then repeating the surface preparation etch, a-Ge deposition, and chromium/gold electrode deposition steps on the front detector surface. The detector fabrication was completed by removing the back-side cement mask with trichloroethylene. The detector was then placed into an aluminum frame designed so that only the side lobes of the detector contacted the frame. Indium foil was placed between the detector and these contact points. Wire springs covered with teflon were then used to mechanically restrain the detector in the frame. Electrical connection to the detector electrodes was made through ultrasonic wire bonding between the electrodes and the bonding pads on two circuit boards attached to the mounting frame.

The completed and mounted detector was then placed into a test cryostat. The test configuration varied somewhat between the different measurements, however a bias of 1000 V was typically applied to the front-side guard ring and strips while the back-side guard ring and strips were maintained at ground potential. Full depletion of the detector occurred at about 300 V. Induced charge signals from the strip electrodes were measured with ac-coupled charge-sensitive preamplifiers, acquired with a digital oscilloscope, and processed with LabVIEW programs running on a PC. Pulse-height spectra were also acquired through a standard pulse processing electronics chain.

3. Three-dimensional position sensing

The location of each gamma-ray interaction event in the position-sensitive volume of the detector shown in Figure 1 can in principle be determined in three dimensions. The location in

the directions parallel to the detector contacts (x and y directions) is simply given by the positions of the strip electrodes that collect the charge generated by the interaction event. In this detector, the electrons generated by an interaction event drift and are collected by the front-side electrodes, and the generated holes are collected by the back-side electrodes. The front-side electrode(s) that collects the electron charge indicates the interaction location in the x direction, and the back-side electrode(s) that collects the holes gives the y location. An example of this position detection is given in Figure 2. Here we show the results from scanning a collimated ^{241}Am gamma-ray source (59.5 keV) along the middle electrode of the front-side surface while measuring the charge collection events on the back-side electrodes. For this measurement, alternate back-side electrodes were connected together (in order to minimize the number of readout channels required for the test), and pulse-height spectra were accumulated from the resulting two sets of back-side electrodes. Plotted in Figure 2 is the number of counts within the photopeak of the spectra acquired from these back-side electrodes as a function of the source location. As the source is scanned and the resultant electron collection moves from one back-side electrode to the next, the photopeak counts from each of the two electrode sets is observed to rise or fall as expected thereby demonstrating good y position sensitivity. Likewise, the front-side electrodes behave similarly for the measurement of the event location in the x direction.

The determination of the depth of interaction (z location) for a gamma-ray interaction event can be made based on the time difference in the electron arrival at the anode and the hole arrival at the cathode. For a simple non-segmented planar geometry detector, this detection scheme can be problematic. First of all, the collection of the charge generated by a gamma-ray interaction event produces an induced charge on the planar electrodes that is simply proportional to the separation of the drifting electron and hole charges. At the start of the collection process in such a detector, the induced charge will rise linearly in time. This continues until either the electrons or the holes are collected at one of the detector electrodes, at which point the rate of rise drops by about 50 % since only the other polarity of charges will be drifting within the detector. This continues until finally the remaining drifting charge is collected at the opposing detector electrode. The measurement of the time differences between the start, the slope change, and the stop of the induced charge signal rise must be made in order to determine the interaction depth of the gamma ray. However, the extraction of accurate timing information from the slope change can be difficult in practice as a result of noise. Another more fundamental problem is

determining whether the slope change is a result of hole collection at the cathode or electron collection at the anode. The change in pulse slope during the drift process could be a result of either charge type being collected. Therefore, an interaction event that is a specific distance from the cathode will produce nearly the same induced charge signal as an event that occurs the same distance from the anode. This is because the drift velocity of the electrons is close to that of the holes in Ge. Consequently, there is an ambiguity in determining the depth of interaction from the induced charge signals in simple planar geometry Ge detectors.

The situation is different in the orthogonal-strip detector because of a small-electrode effect [14-16]. Consider a gamma-ray interaction event taking place near the center of the detector shown in Figure 1. Under the influence of the applied bias, the generated carriers drift and separate. However, in contrast to the simple planar detector geometry, little charge is initially induced on the particular front-side and back-side strip electrodes that will eventually collect the electrons and holes (referred to as electron-collecting electrode and hole-collecting electrode, respectively). This is because the nearby electrode strips and guard ring on both sides of the detector act to partially screen the collecting electrodes from the drifting carriers. This changes when the drifting charge moves into close vicinity of a collecting electrode. At this point there is a rapid rise in the induced charge on that particular electrode which continues until the drifting charge is fully collected on the electrode. The rapid rise in the induced charge signal on the electron-collecting electrode marks the arrival of the electrons at that electrode, and likewise the rapid signal rise on the hole-collecting electrode marks the arrival of the holes. The key element here is that the collection of the electrons and the collection of the holes are each separately detected. The difference in the arrival times for these two signals can then be used to determine the depth of the gamma-ray interaction. For example, if the arrival of the electrons occurs prior to that of the holes, the interaction event must have taken place closer to the electron-collecting electrode; whereas if the opposite is true, the event must have occurred closer to the hole-collecting electrode.

As an illustration of this depth of interaction sensing technique, we show in Figures 3 and 4 modeling results for a detector with a geometry approximate to that shown in Figure 1. In this simple model, photoelectric gamma-ray interaction events were assumed to occur in the center (x and y directions) of the overlap region between the front-side electrode x_3 and the back-side electrode y_3. The free electrons and holes generated by each event were then assumed to drift in

straight trajectories to the appropriate electrodes as governed by the detector field and the field dependent drift velocities. With these assumptions, the induced charge signals on the charge-collecting electrodes were calculated using the weighting potential method [18,19]. This calculation was made for interaction events occurring at several different depths z_o from the front-side electron-collecting electrode x_3, and the resulting induced charge signals are shown in Figure 3. As expected, the relative timing of the pulses on the electrodes is dictated by the interaction depth. An event taking place near the front-side electrode (small z_o value) produces a rapidly changing charge pulse on the front-side electrode prior to the corresponding pulse on the back-side electrode, whereas the opposite is true for an event occurring near the back-side electrode (large z_o value). Finally, for an event near the middle of the detector, the pulses nearly coincide in time. In Figure 4 the interaction depth is plotted as a function of the calculated time difference between the occurrence of the pulse on the front-side electrode and that on the back-side electrode. For simplicity each pulse location was taken to be the time when the pulse reached its half-maximum magnitude value. Over nearly the entire detector depth there is a one-to-one near-linear relationship between the depth of interaction and the pulse time separation. This shows that the gamma-ray interaction depth can in principle be easily extracted from the time separation of the pulses. The only regions in the detector where this becomes difficult are locations that are very near either of the electrodes. Within these *near-electrode* regions (within the distance of about one-half the center-to-center strip distance) the pulse time separation changes little with the gamma-ray interaction depth. To understand this, consider the collection of charge generated by an interaction event occurring at the electron-collecting electrode, $z_o = 0$. The generated electrons are immediately collected by this electrode and consequently do not contribute to the induced charge signal on the electrode. The charge induction on this electrode is then solely a result of the drift of the holes out of this near-electrode region. In contrast to this is an event that occurs slightly deeper in the detector yet still within the near-electrode region, $z_o = \Delta z$. For this event, both the drift of the electrons and the holes within the near-electrode region contribute to the induced charge signal on the electron-collecting electrode. The signal increases as the separation between the electrons and holes increases. Since in this case both the electrons and the holes are drifting, the pulse will rise faster than in the case of the $z_o = 0$ event in which only the holes are drifting. The electron-collecting electrode signal will actually reach its half-maximum pulse-height value at a time earlier for the $z_o = \Delta z$ event than for the $z_o = 0$ event.

Since the half-maximum value of the hole-collecting electrode signal for the $z_o = \Delta z$ event will also occur at a time earlier than that of the $z_o = 0$ event, there will be little difference in the pulse time separation for the two events. The impact of this near-electrode effect can however be lessened by reducing the near-electrode region through the choice of a finer electrode spacing or perhaps through more sophisticated pulse-timing measurements.

We have experimentally investigated this depth of interaction sensing method using our prototype orthogonal-strip detector. A set of induced charge signals obtained from the detector is shown in Figure 5. The signals are those from the x_3 and y_3 electrodes. Each pulse pair shown results from the collection to these electrodes of the charge generated by a gamma ray from a ^{57}Co source (122 keV) placed in front of the front-side detector surface. This set of measured pulse pairs matches well with the calculated ones of Figure 3 in terms of the variation and magnitude of the time separation between the pulse pairs. The measured pulse shapes are, however, limited by the finite response time of the preamplifiers used and therefore do not exhibit the very sharp rise seen in the calculated waveforms. To confirm experimentally that the time separation between each corresponding x_3 pulse and y_3 pulse relates to the gamma-ray interaction depth, we have acquired time spectra with the detector when separately exposed to ^{241}Am, ^{57}Co, and ^{137}Cs (661.6 keV) gamma-ray sources. The spectra were each obtained by repeatedly doing the following: acquiring a pulse pair, measuring the time difference between the occurrence of the x_3 pulse-height half-maximum and the occurrence of the y_3 pulse-height half-maximum, and incrementing the count in the channel number corresponding to the measured time difference. The pulse pairs were acquired using a digital oscilloscope and then transferred to a PC and analyzed in real time using LabVIEW. The threshold for triggering an acquisition event during this process was set to about 15 keV for both electrode signals. Spectra gathered using this technique are shown in Figure 6. The bottom axis of these plots represents the y_3 pulse location in time subtracted from the x_3 pulse location. Therefore, negative time differences of about -100 ns correspond to gamma rays that interacted near the front-side x_3 electrode, whereas time differences of about 100 ns resulted from events near the back-side y_3 electrode. The measured time distributions clearly depend on the energy of the incident gamma rays. As expected, the lower energy gamma rays predominantly produced events near the entrance (front) side of the detector (Figure 6a), whereas the higher energy gamma rays led to a more uniform distribution of the events with depth (Figure 6c). Each of these distributions can be compared to

the simple exponential attenuation of the gamma-ray intensity with depth. Using attenuation coefficients appropriate for the specific gamma-ray energies [20], we have calculated the expected distributions and superimposed them onto the spectra of Figure 6. For simplicity, we have assumed here a linear relation between the depth of interaction and the measured time difference. The measured and calculated distributions are in good agreement with each other, thus confirming the accuracy of this technique. The depth position resolution achieved with this technique will in part be limited by the electronic noise of the electrode signals. To quantify this contribution to the position resolution broadening, we simultaneously applied a periodic electronic pulse signal to both the x_3 electrode and the y_3 electrode and then accumulated a time spectrum. A pulse height corresponding to that of a 59.5 keV gamma-ray event was used. The resulting spectrum shown in Figure 6d has a peak with a width of 4.4 ns. This corresponds to a depth position resolution of about 0.25 mm and illustrates that in principle highly accurate depth sensing can be achieved even for relatively low energy events.

We note that this method of depth of interaction measurement was also recently demonstrated by Momayezi [21].

4. Charge collection and field shaping

Segmenting a detector contact in order to enable position readout, such as dividing the detector cathode and anode into strips, can degrade the performance of a detector. This degradation can be a loss of both energy resolution and photopeak efficiency. One of the primary physical causes of the degraded performance is the existence of weak lateral electric field regions between adjacent electrode segments. As an illustrative example, consider the case of a gamma ray interacting between electrodes y_2 and y_3 of the detector in Figure 1. The electric field set up in the detector by the positive bias applied to the front-side electrodes causes the generated holes to drift towards the y_2 and y_3 electrodes. However, since both electrodes are at the same potential, it is not clear what will happen to the holes when they drift near the two strips. One possibility is that the potential of the detector surface between the two electrodes is more positive than the electrodes. In this case the charge could potentially be efficiently collected to the electrodes. The drifting charge will then be shared between the y_2 and y_3 electrodes, and the full energy signal can be recovered by summing together the two individual

electrode signals [22]. No loss of detector performance would result for this ideal charge sharing situation. Another possibility, though, is that little or no lateral (y direction) electric field exists to cause the holes to be completely collected by the electrodes within the pulse measurement time. In this case the holes would be collected efficiently to the detector surface between the two electrodes but then only slowly collected the remaining distance to the electrodes. Since the holes may not be completely collected to the electrodes within the pulse measurement time, even the summed signal will have a deficit. A loss of either or both energy resolution and photopeak efficiency will be the result.

To determine which of these situations exists in our prototype detector, we have analyzed the detector response to events occurring between electrodes. This was accomplished by probing the front side of the detector with a finely collimated ^{241}Am gamma-ray source while acquiring induced charge signal data from the back-side electrodes. The gamma-ray source used produced a beam about 0.5 mm in diameter and was mounted on a x-y translation stage so that the detector response could be measured as a function of the gamma-ray interaction location. To reduce the number of readout channels required for this measurement, alternate back-side electrodes were connected together. For a reason that will become clear later, the interconnected electrodes y_2 and y_4 will be referred to as field electrodes and the electrodes y_1, y_3, and y_5 as sensing electrodes. The source was then scanned in the y direction while monitoring the signals on these two sets of electrodes in order to position the source between electrodes y_2 and y_3. At this source location, the pulse height measured at the field-electrode readout channel is mainly a result of the charge induction on the y_2 electrode while the pulse height measured at the sensing-electrode readout channel results primarily from the charge induction on the y_3 electrode. The pulse height from either of these channels is roughly proportional to the relative location of the gamma-ray event between y_2 and y_3. This pulse-height information was accumulated for events that produced coincidence pulses on the two readout channels. The result of this measurement is shown in Figure 7 where the summed pulse height (of the field and sensing electrodes) is plotted against the field-electrode pulse height. Each dot in the plot then represents a single gamma-ray interaction event in the detector that led to charge sharing between the y_2 electrode and the y_3 electrode. For the ideal charge-sharing situation, the summed pulse height should always correspond to the gamma-ray energy of 59.5 keV. This, however, is not the case here. When the induced charge signal is shared between the two sets of electrodes, a pulse-height deficit is

observed in the summed signal. This deficit is a maximum when the two sets of electrodes equally share the signal presumably as a result of an event occurring midway between the y_2 and y_3 electrodes.

Using a simple model of the detector, we can determine if this result is consistent with the idea of charge collection to the surface between the two electrodes. In this model the electrons generated by each gamma-ray interaction event are assumed to be fully collected by the front-side electrodes and the holes fully collected to the surface between the y_2 electrode and the y_3 electrode. The electron and hole charge clouds are also assumed to be point-like in this calculation. We are therefore neglecting the effects caused by the finite size of the initially generated charge clouds and the subsequent spreading by diffusion [23]. With these assumptions, we have calculated the total induced charge pulse height from the field and sensing electrodes as a function of the pulse height from field electrodes alone using the weighting potential method [18,19]. The result of the calculation is the solid line plotted in Figure 7. The calculated response matches reasonably well with the measured data and predicts a maximum charge collection deficiency of about 5 %. Based on the above measurements and this modeling result, it is apparent that incomplete charge collection resulting from a weak lateral electric field between electrodes is present. Left uncorrected this will lead to degraded detector performance.

One method to overcome this problem is to introduce a potential difference between adjacent electrodes. This can be accomplished by using only every other electrode for signal readout. These charge-sensing electrodes would each be connected to a separate readout channel. The remaining strip electrodes would then be interconnected to act as field-shaping electrodes. Through the application of an appropriate bias between the field electrodes and the sensing electrodes, the weak lateral electric field at the detector surface can be eliminated, thereby enabling complete charge collection to the sensing electrodes. Such a detection scheme would be difficult to implement, though, with the conventional boron-implanted (p^+) or lithium-diffused (n^+) contact technologies used with Ge detectors. These contacts are either non-injecting for electrons or for holes but not for both. Consequently, the application of the necessary bias between two adjacent boron-implanted strips, for example, would lead to a substantial leakage current as a result of hole injection at the positively biased strip. Alternate p^+ and n^+ contacts would have to be produced to avoid this problem. A considerable advantage of the amorphous

semiconductor contacts is that they do not suffer from this limitation. These contacts can exhibit good blocking behavior under either bias polarity.

Since our prototype detector was produced with amorphous semiconductor contacts, we were able to test the field-shaping scheme just described. To determine the effectiveness of using field-shaping electrodes, the detector was connected and tested in the same manner as that used to obtain the results of Figure 7. The only addition was that of a negative bias V_s applied to the sensing electrodes. The results of measurements at three different sensing-electrode biases are shown in Figure 8. This figure shows that with the addition of V_s, the dip in the distribution of the events, which indicates a pulse-height deficit (Figure 8a), can be largely eliminated by forcing complete collection at the sensing electrodes (Figure 8c). This then improves the detector performance as the spectroscopic measurements of Figures 9 and 10 demonstrate. Each spectrum in these figures was acquired by placing a gamma-ray source facing the front side of the detector and measuring the signals from the individual sensing electrode y_3. The measurements were made with this electrode and the other back-side sensing electrodes at a bias V_s, the back-side field electrodes and guard ring grounded, and all the front-side electrodes at 1000 V. From the ^{241}Am spectra of Figure 9, we see that the application of a -200 V sensing-electrode bias substantially increased the counts in the photopeak by allowing the charge from events within the inter-electrode regions and beneath the nearby field electrodes to be fully collected. The background counts were also reduced as a result of a decrease in the number of events with incomplete charge collection. Additionally the application of the sensing-electrode bias did not measurably increase the electronic noise as the pulser widths indicate, and the energy resolution at 59.5 keV improved slightly. The ^{137}Cs spectra of Figure 10 further demonstrate the performance improvements achieved with this technique.

5. Summary

We have fabricated a prototype 5×5 orthogonal-strip Ge detector with amorphous-semiconductor contacts. This detector was used in part to better understand the processes that can degrade the performance of such detectors for imaging applications and to develop techniques to overcome the problems. With this detector we demonstrated that not only could the location of each gamma-ray interaction event be determined in the directions parallel to the

contact surfaces but that the depth of the event could be measured. This depth measurement is based on the difference in the arrival of the gamma-generated holes at the cathode strips and the arrival of the electrons at the anode strips. Ultimately, this more accurate measurement of the interaction location (in all three dimensions instead of only two) should improve the image quality achieved with these detectors.

We also established that the segmented electrode structures used for position detection in this type of detector could lead to a loss of energy resolution and photopeak efficiency. This degraded performance is caused by the incomplete collection of the charge generated by gamma-ray interaction events occurring in the gap regions between electrodes. A model in which the generated charge is only collected to the detector surface and not completely to the electrodes during the pulse measurement time was shown to match well with the measured data. With this detector we were able to substantially overcome this problem by implementing a field-shaping electrode between each charge-sensing electrode on the detector. With the appropriate application of bias between the field electrodes and the sensing electrodes, efficient charge collection to the sensing electrodes was produced. This then significantly improved the detector performance in terms of a reduced background and increased photopeak efficiency.

Acknowledgements

We thank J. S. Lee for her careful editing of the manuscript.

References

[1] R. P. Parker, E. M. Gunnersen, J. L. Wankling, and R. Ellis, Medical Radioisotope Scintigraphy, International Atomic Energy Agency, Vienna, 1969, p. 71.

[2] J. F. Detko, Medical Radioisotope Scintigraphy, International Atomic Energy Agency, Vienna, 1973, p. 241.

[3] P. A. Schlosser, D. W. Miller, M. S. Gerber, R. F. Redmond, et al., IEEE Trans. Nucl. Sci. NS-21 (1974) 658.

[4] L. Kaufman, V. Lorenz, K. Hosier, J. Hoenninger, et al., IEEE Trans. Nucl. Sci. NS-25 (1978) 189.

[5] D. Miller, P. Schlosser, A. Deutchman, J. Steidley, et al., IEEE Trans. Nucl. Sci. NS-26 (1979) 603.

[6] P. N. Luke, IEEE Trans. Nucl. Sci. NS-31 (1984) 312.

[7] D. Protic and G. Riepe, IEEE Trans. Nucl. Sci. NS-32 (1985) 553.

[8] D. Gutknecht, Nucl. Instr. and Meth. A 288 (1990) 13.

[9] A. Hamacher, H. Machner, M. Nolte, M. Palarczyk, et al., Nucl. Instr. and Meth. A 295 (1990) 128.

[10] P. N. Luke, R. H. Pehl, and F. A. Dilmanian, IEEE Trans. Nucl. Sci. NS-41 (1994) 976.

[11] P. N. Luke, M. Amman, B. F. Phlips, W. N. Johnson, et al., submitted to IEEE Trans. Nucl. Sci.

[12] W. L. Hansen and E. E. Haller, IEEE Trans. Nucl. Sci. NS-24 (1977) 61.

[13] P. N. Luke, C. P. Cork, N. W. Madden, C. S. Rossington, et al., IEEE Trans. Nucl. Sci. NS-39 (1992) 590.

[14] H. L. Malm, C. Canali, J. W. Mayer, M-A. Nicolet, et al., Appl. Phys. Lett. 26 (1975) 344.

[15] H. H. Barrett, J. D. Eskin, and H. B. Barber, Phys. Rev. Lett. 75 (1995) 156.

[16] P. N. Luke, Nucl. Instr. and Meth. A 380 (1996) 232.

[17] H. L. Malm and R. J. Dinger, IEEE Trans. Nucl. Sci. NS-23 (1976) 76.

[18] W. Shockley, J. Appl. Phys. 9 (1938) 635.

[19] S. Ramo, Proc. I.R.E. 27 (1939) 584.

[20] M. J. Berger and J. H. Hubbell, XCOM: Photon Cross Sections Database, National Institute of Standards and Technology, Gaithersburg, 1998.

[21] M. Momayezi, W. K. Warburton, and R. Kroeger, SPIE 3768 (1999) 530.

[22] G. Rossi, J. Morse, and D. Protic, IEEE Trans. Nucl. Sci. NS-46 (1999) 765.

[23] R. A. Kroeger, N. Gehrels, W. N. Johnson, J. D. Kurfess, et al., Nucl. Instr. and Meth. A 422 (1999) 206.

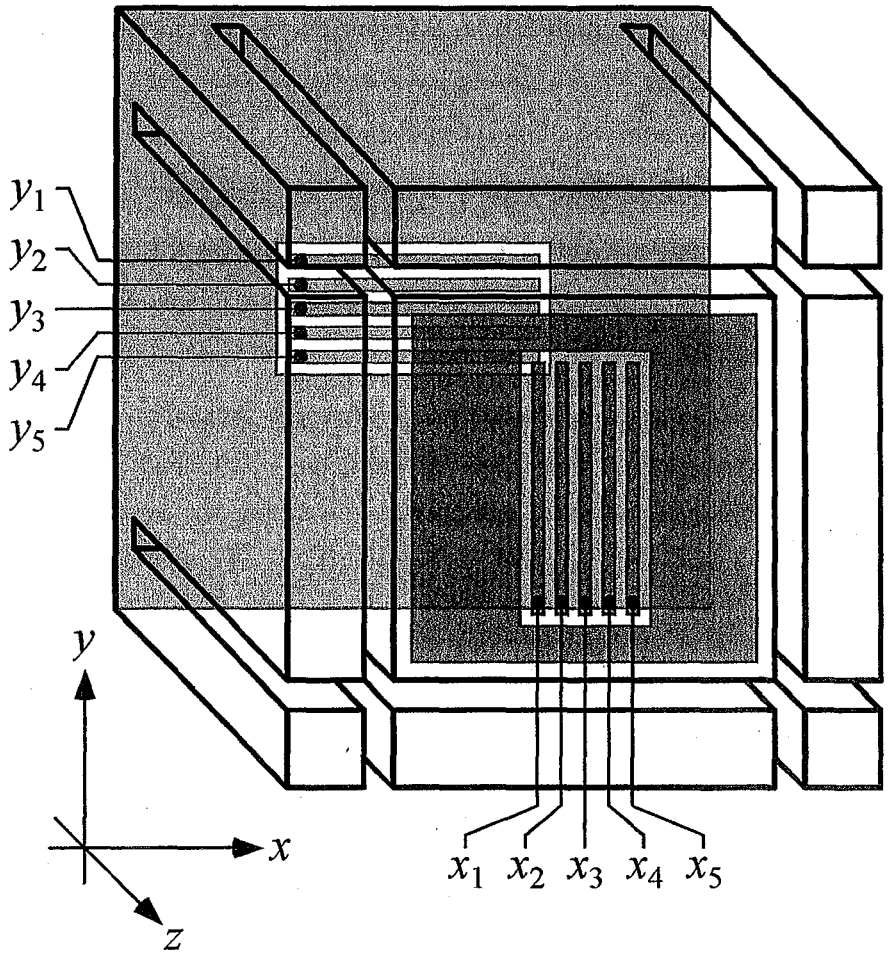

Figure 1. Schematic diagram of a prototype orthogonal-strip Ge detector for gamma-ray spectroscopy and imaging. The position-sensitive volume of this detector is formed by the overlap of the five x position electrode strips on the front side of the detector and the five y position electrode strips on the back side of the detector.

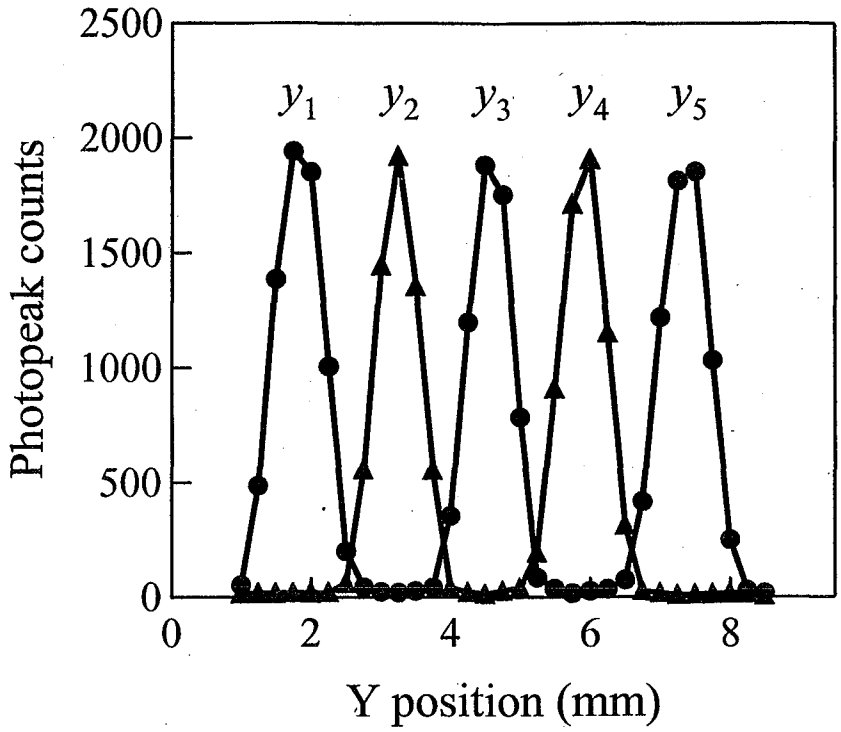

Figure 2. Integrated counts within the photopeak as a function of the collimated ^{241}Am gamma-ray source location measured with the prototype orthogonal-strip detector schematically shown in Figure 1. The source with a beam diameter of about 0.5 mm was scanned in the y direction along the front side of the detector while the pulse-height information was acquired from the back-side electrodes. Alternate back-side electrodes were interconnected for this test measurement so that only two readout channels would be necessary. The energy window for the integration was from 56.5 keV to 62.5 keV.

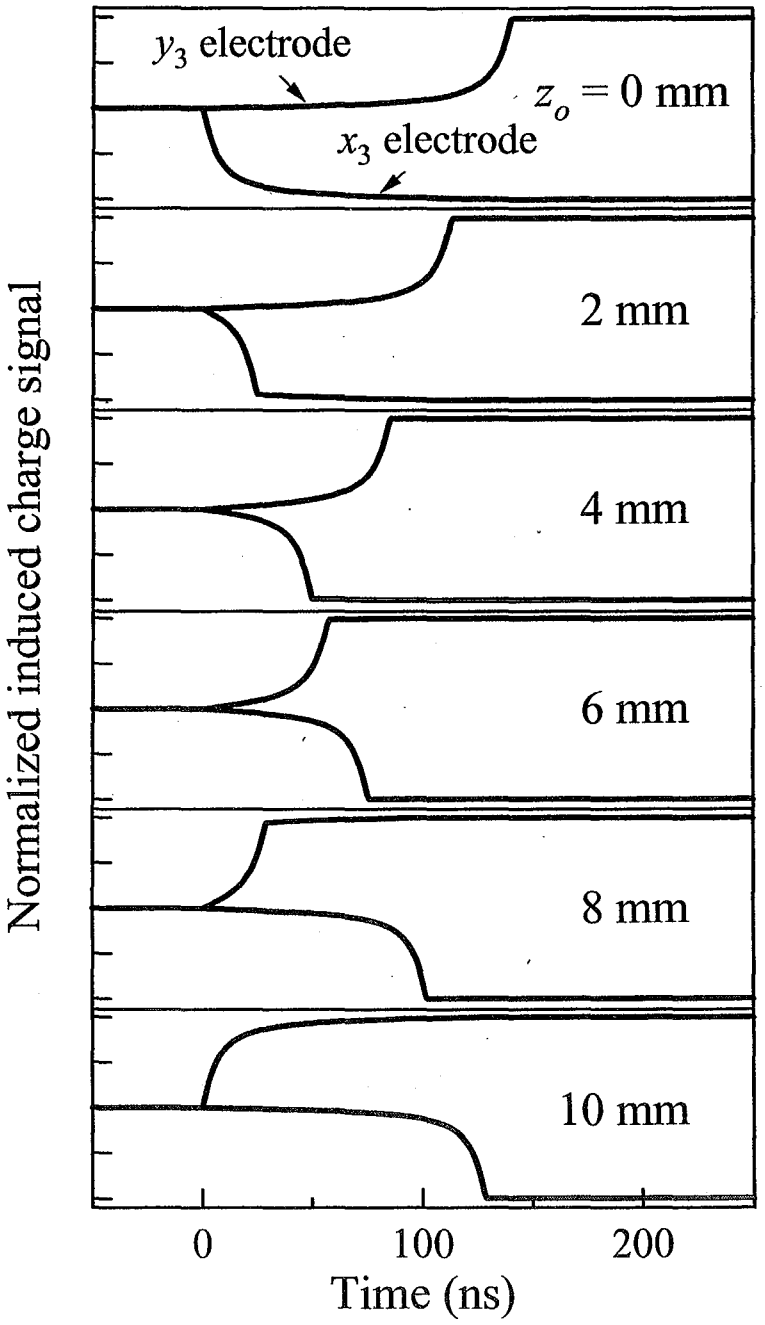

Figure 3. Calculated induced charge signals from the x_3 electrode and the y_3 electrode of the prototype orthogonal-strip detector schematically shown in Figure 1. Each pulse pair shown results from the collection of the charge generated by a photoelectric gamma-ray interaction event occurring at a different depth z_o from the front side of the detector. This illustrates that the time difference between the occurrence of the front-side strip pulse and the back-side strip pulse can be used as a measure of the gamma-ray interaction depth.

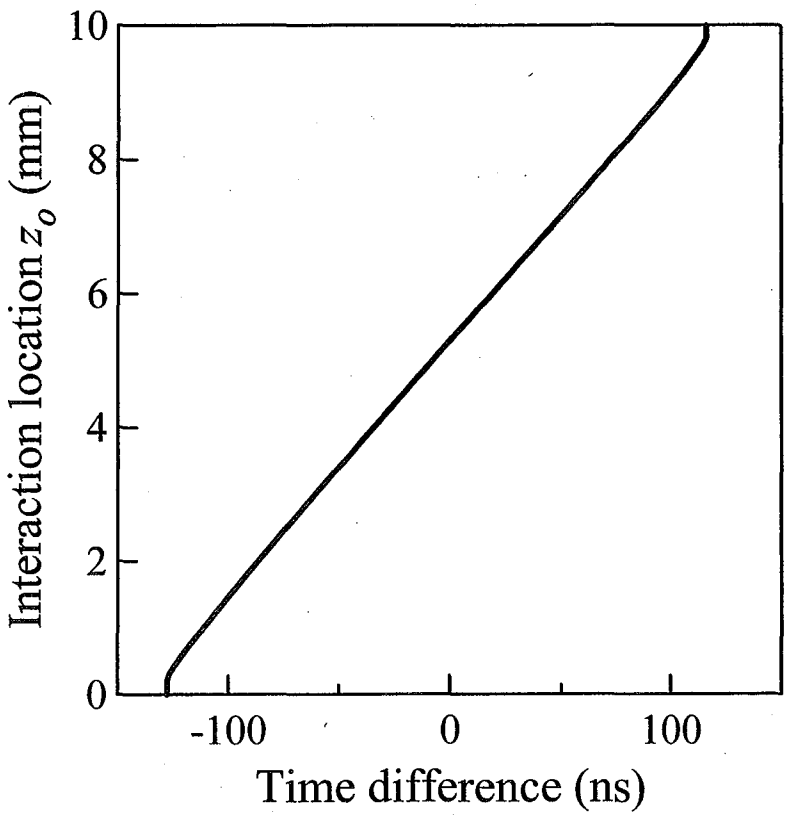

Figure 4. Gamma-ray interaction depth plotted as a function of the calculated time difference between the resultant x_3 electrode pulse and the y_3 electrode pulse for the prototype orthogonal-strip detector. The location of each pulse was taken to be the time at which the pulse reached its half-maximum magnitude value.

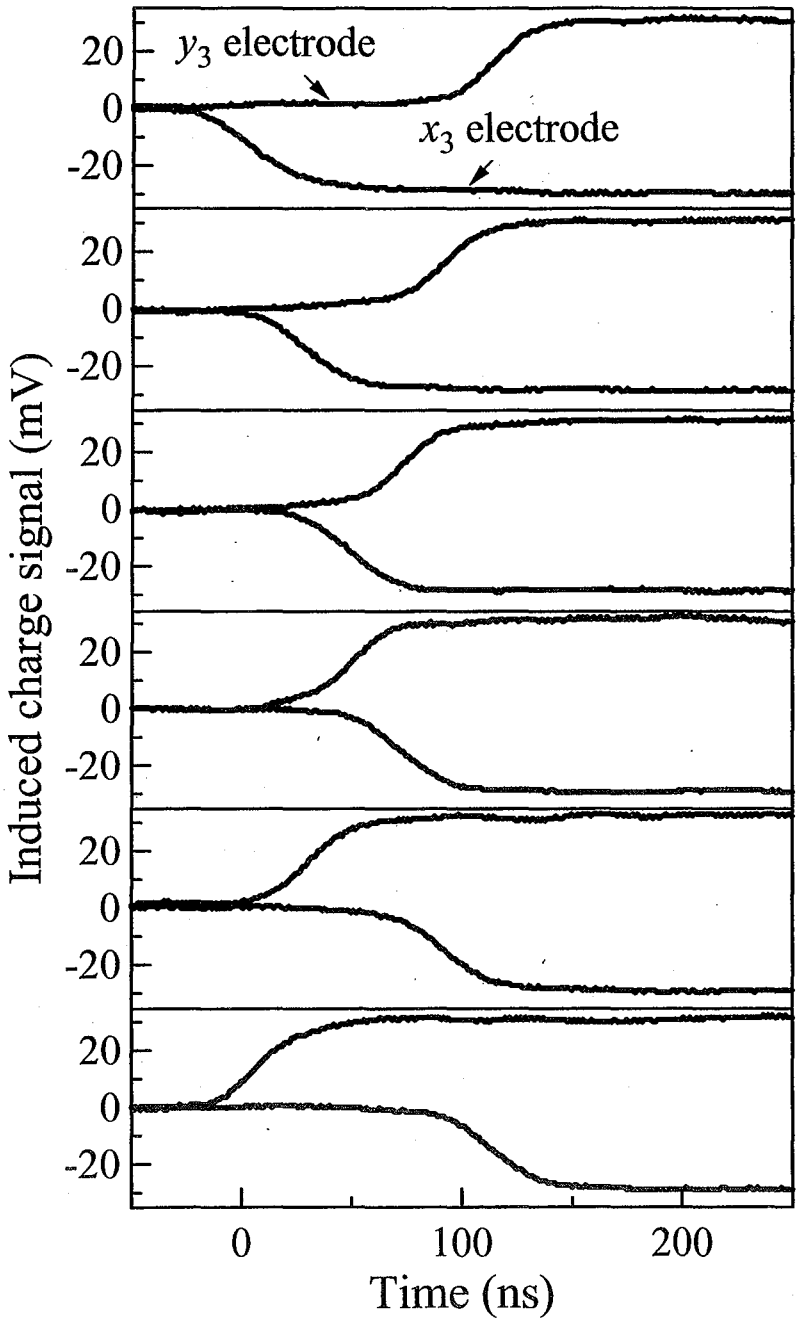

Figure 5. Measured induced charge signals from the x_3 electrode and the y_3 electrode of the prototype orthogonal-strip detector schematically shown in Figure 1. Each pulse pair shown results from the collection of the charge generated in the detector by a gamma-ray from a ^{57}Co source. This set of measured pulses is comparable to the calculated pulses of Figure 3.

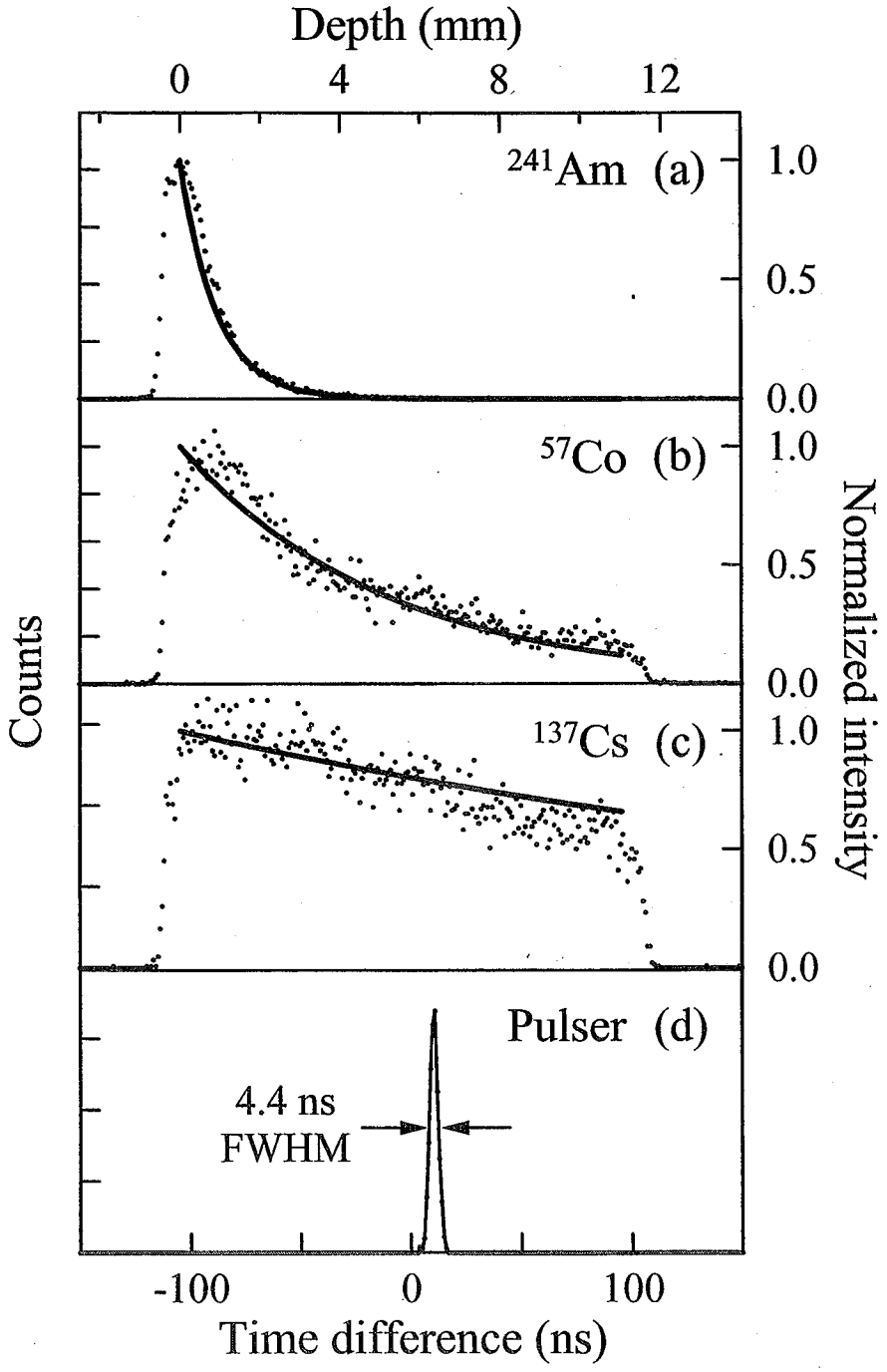

Figure 6. Time spectra acquired with the prototype orthogonal-strip detector. Each spectrum was produced by repeatedly acquiring a coincidence pulse pair from electrodes x_3 and y_3, measuring the time difference between the x_3 electrode pulse and the y_3 electrode pulse, and then incrementing the channel number in the spectrum corresponding to the measured time difference. The location of each pulse was taken to be the time at which the pulse reached its half-maximum magnitude value. A separate time spectrum (dots) was measured for each of the following

sources placed in front of the detector: (a) ^{241}Am, (b) ^{57}Co, and (c) ^{137}Cs. For comparison the expected exponential decay in the intensity of the gamma rays with depth (solid lines) is superimposed on top of the measured spectra. A time spectrum acquired when periodic electronic pulse signals were simultaneously applied to the x_3 and y_3 electrodes is plotted in (d). The pulse height used corresponds to a 59.5 keV gamma-ray event. The width of the peak in this spectrum is a measure of the uncertainty in the depth determination introduced by the noise of the measurement electronics.

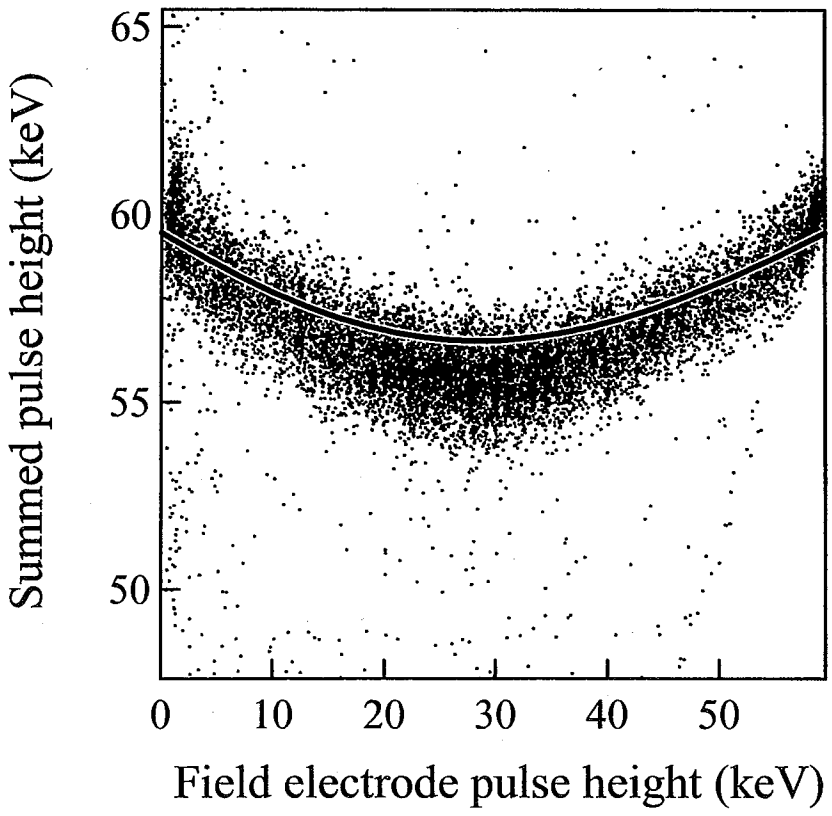

Figure 7. Scatter plot of measured gamma-ray interaction events that occurred in the gap between electrodes y_2 and y_3 of the prototype orthogonal-strip detector. This data was acquired by positioning a collimated ^{241}Am gamma-ray source in front of the detector and measuring the induced charge pulses from the back-side y electrodes interconnected into field (y_2 and y_4) and sensing (y_1, y_3, and y_5) electrode sets. For each event the summed energy from the field and sensing electrodes is plotted against the energy from the field electrodes. The dip in the distribution indicates a pulse-height deficit for events occurring in the gap between y_2 and y_3. For comparison the calculated total pulse height as a function of the pulse height from the field electrodes is plotted (solid line). These pulse heights were determined by assuming that the generated holes were collected directly to the detector surface between electrodes y_2 and y_3 and not completely to either electrode.

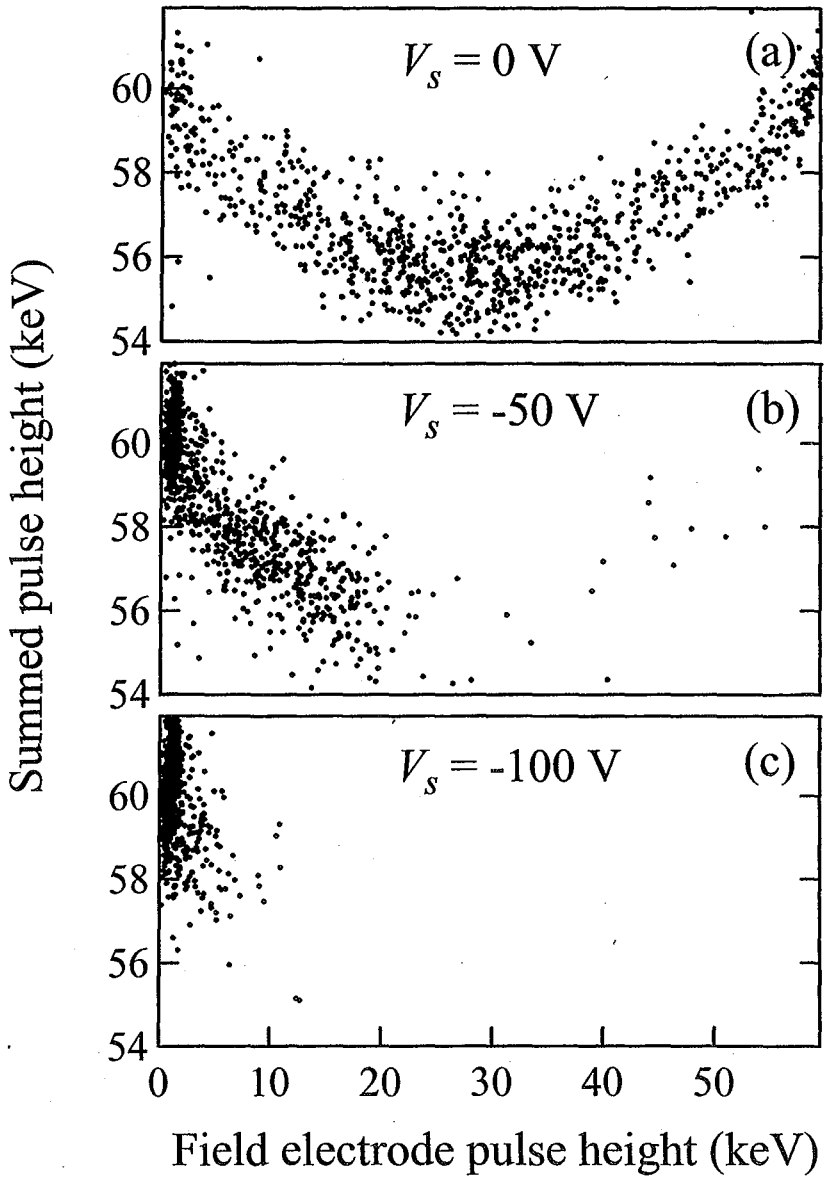

Figure 8. Scatter plots of measured gamma-ray interaction events that occurred in the gap between electrodes y_2 and y_3 of the prototype orthogonal-strip detector. This data was acquired in the same manner as that of Figure 7 except that in this case a bias V_s was applied to the sensing electrodes. The sensing-electrode biases used to obtain the plots were (a) 0 V, (b) -50 V, and (c) -100 V. This sensing-electrode bias can substantially eliminate the dip in the scatter plot distribution by forcing a more complete collection of the charge to the sensing electrodes.

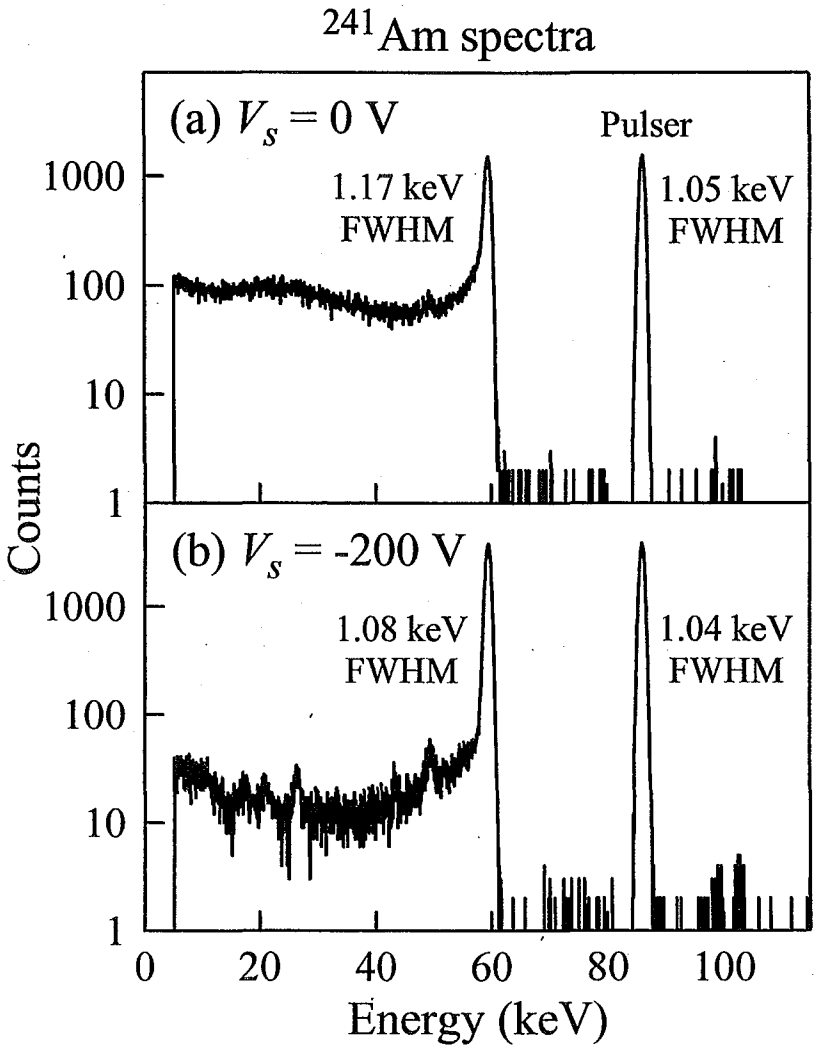

Figure 9. ^{241}Am pulse-height spectra acquired from the back-side y_3 electrode of the prototype orthogonal-strip detector. The source was placed facing the front-side of the detector for this measurement. The electrodes y_2 and y_4 were interconnected and used as field electrodes by connecting them to ground potential. The sensing electrodes y_1, y_3, and y_5 were all held at the potential V_s and isolated from each other so that signals could be measured from each one separately. A spectrum was measured without the addition of field shaping, (a) $V_s = 0$ V, and with the added benefit of field shaping, (b) $V_s = -200$ V.

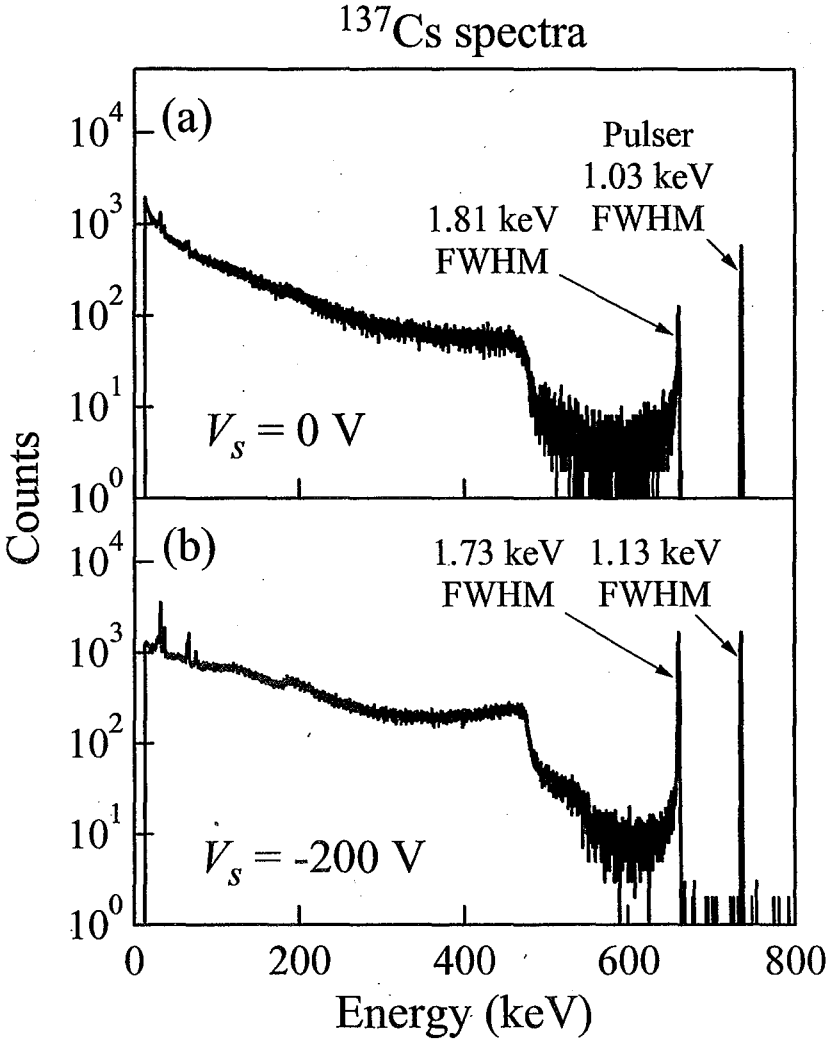

Figure 10. ^{137}Cs pulse-height spectra acquired from the back-side y_3 electrode of the prototype orthogonal-strip detector. The source was placed facing the front-side of the detector for this measurement. The electrodes y_2 and y_4 were interconnected and used as field electrodes by connecting them to ground potential. The sensing electrodes y_1, y_3, and y_5 were all held at the potential V_s and isolated from each other so that signals could be measured from each one separately. A spectrum was measured without the addition of field shaping, (a) $V_s = 0$ V, and with the added benefit of field shaping, (b) $V_s = -200$ V.